RESIDUAL STRESS MEASUREMENTS IN MULTICRYSTALLINE SILICON BULK AND THIN FILM SOLAR CELLS USING MICRO-RAMAN SPECTROSCOPY

G. Sarau[1,2,*], M. Becker[1,2], G. Andrä[2], S. Christiansen[1,2]
[1]Max-Planck-Institute of Microstructure Physics, Weinberg 2, D-06120 Halle, Germany
[2]Institute of Photonic Technology, Albert-Einstein Str. 9, D-07745 Jena, Germany
[*]Correspondence: Tel: +49 3641 206401, Fax: +49 3641 206499, E-mail: gsarau@mpi-halle.de

ABSTRACT: Residual mechanical stress is currently among the most important parameters for improving processing yields and it will become increasingly important in view of the targeted decrease in the wafer or thin film thicknesses to reduce processing costs. A technique that is intensively used for analysing stress states at the micrometer scale in semiconductors is micro-Raman spectroscopy. Several stress-tensor components can be obtained separately using polarized laser light for the μ-Raman measurements or average stresses when using unpolarized light. We have found inhomogeneous stress distributions including local peak compressive and tensile stresses at (sub)grain boundaries and in areas with high concentrations of extended lattice defects. These stresses most probably form during the different heating and cooling processes of the multicrytalline silicon block and ribbon casting or during the laser melting and re-crystallization of amorphous silicon layers on thermally mismatched glass substrates. The possible mechanisms of stress formation and relaxation are discussed.
Keywords: Stress, Raman, Multicrystalline Silicon, Thin Film, Defects, Dislocation, Grain Boundary.

1 INTRODUCTION

Residual stresses are stresses which are retained in the solar cell material when no external forces are applied. These internal stresses may combine critically with external loads (mechanical, thermal) or unfavourable assembly of pre-existing extended lattice defects (microstructure) resulting in unexpected cell breakage [1]. Moreover, they may induce the formation of new extended lattice defects such as dislocations and low-angle grain boundaries which often act as recombination sites for minority carriers in a solar cell as well as initiation points for cracks that all together degrade performance and aesthetics of the solar cell. Therefore, in addition to electrical and optical properties, the knowledge of the origin, spatial distribution and values of residual mechanical stresses is of key importance for optimizing solar cell parameters and essentially process yields.

In the present study micro-Raman spectroscopy was used to detect residual stress fields at the micrometer scale in multicrytalline (mc) silicon solar cells based on block-cast and edge-defined film-fed growth (EFG) wafers and layered laser crystallized (LLC) thin films on glass [2]. These investigations were performed at (sub)grain boundary assemblies and in highly defective areas within a grain close to the defects that were made visible by defect etching. In some cases we have evaluated not only the average stresses but several stress-tensor components separately by means of polarized μ-Raman spectroscopy [3]. The origin of the measured stresses is discussed by considering the possible mechanisms of stress formation and relaxation in the solar cell materials during thermal processing.

2 EXPERIMENTAL DETAILS

The block-cast and EFG wafers are commercially available material, while the LLC thin films on glass are prepared at IPHT, Jena [2]. To assure stress measurements by Raman spectroscopy that are not influenced by uncontrolled reflections at rough surface facets, the silicon surfaces are planarized by mechanical polishing. Then, the samples are Secco-etched [4] for 5 – 30 s to reveal grain boundaries and dislocations.

The Raman measurements are carried out at room temperature in the backscattering configuration using a LabRam HR800 spectrometer from Horiba Jobin Yvon equipped with a Peltier-cooled CCD detector, an 1800 lines/mm grating, a He-Ne laser with an excitation wavelength of 633 nm, an optical microscope and a motorized *x*-*y* stage. The incident laser light is focused onto the sample's surface through a 100x objective resulting in a focused spot with a diameter of 1 - 1.5 μm and a penetration depth of a few μm in silicon. Raman spectra are measured by moving the sample with 0.8 μm steps in *x*- and *y*-directions. By fitting these spectra with a Gauss-Lorentzian function, the shift of the first-order silicon Raman peak caused by internal stresses can be extracted with a resolution of ~ $\pm$0.05 cm^{-1} [3,5]. No shift due to the local heating of the sample by the laser beam was observed. The effect of the thermal instability of the laser or/and the Raman instrument on the silicon peak position was corrected by using one of the plasma lines of a Ne lamp located in the vicinity of the spectrometer's entrance hole [5,6].

Many authors use the following equation deduced for a crystalline silicon [100] plate under biaxial stress [5] as a fast and good estimation of the stress and its sign from the silicon peak shifts:

$$\sigma(\mathrm{MPa}) = -250\,\Delta\omega(\mathrm{cm}^{-1}) \qquad (1)$$

where $\sigma = (\sigma_{xx} + \sigma_{yy})/2$ with the in-plane stress components $\sigma_{xx} = \sigma_{yy}$ referring to the reference coordinate system shown in Figure 1 (a) and $\Delta\omega = \omega_s - \omega_0$ with ω_0 being the peak position of the stress-free state and ω_s the peak position of the stressed state. Using equation 1 and no polarization settings for incident and scattered light an average stress value can be obtained, while several stress-tensor components can be determined using polarized μ-Raman spectroscopy [3]:

$$\sigma = \begin{pmatrix} \sigma_{xx} & \tau_{xy} & 0 \\ \tau_{xy} & \sigma_{yy} & 0 \\ 0 & 0 & \Delta_z \end{pmatrix} \qquad (2)$$

where the component Δ_z includes the residual stress components σ_{zz}, τ_{xz} and τ_{yz}.

The polarized μ-Raman procedure is described in detail in [3] and is summarized in the following. First, the crystallographic grain orientation of an arbitrarily oriented grain is determined by making use of the Raman intensity dependences on the polarization direction of the incident and scattered light and on the crystallographic grain orientation. Second, since the stresses are too small to produce a visible lifting of degeneracy of the three silicon optical phonon frequencies, the polarization settings (incident and scattered light) for which the intensity of one of the three phonon modes dominates the other two are calculated using the previously determined grain orientation. Third, three Raman mappings of the same area are measured for the three polarization settings and the stress-tensor components are calculated numerically from the Raman frequency shifts with respect to a fixed reference coordinate system - the sample stage.

3 RESULTS AND DISCUSSIONS

Local residual stress fields at critical positions such as (sub)grain boundary assemblies, a grain boundary triple point, a high defective area within a grain, a grain boundary separating a grain from a region of twin lamellas and a grain boundary accompanied by dislocations were investigated by micro-Raman spectroscopy. Inhomogeneous stress distributions including both compressive and tensile stresses were often found in those areas. Since we could not confirm the absence of submicron silicon oxide and multi-metal precipitates such as those described in [7], their influence on the stress states of the grain boundaries can not be ruled out.

3.1 Block-cast mc silicon wafers

Figure 1 (a) shows an optical image of an assembly of subgrain boundaries located in the same grain as confirmed by the Raman intensity mapping (not shown). Stress measurements using polarized μ-Raman were performed in the region enclosed by the white rectangle resulting in the following difference stress tensors referring to the coordinate system shown in Figure 1 (a):

$$\Delta\sigma_1 = \begin{pmatrix} -57\pm10 & -29\pm3 & 0 \\ -29\pm3 & -56\pm10 & 0 \\ 0 & 0 & -24\pm9 \end{pmatrix} \text{ MPa,}$$

$$\Delta\sigma_2 = \begin{pmatrix} -36\pm10 & -4\pm2 & 0 \\ -4\pm2 & -35\pm10 & 0 \\ 0 & 0 & -31\pm9 \end{pmatrix} \text{ MPa.}$$

From the values of the stress-tensor components one can see that the spatial distribution of the stress differs for the two positions. This is confirmed by the Raman mapping displayed in Figure 1 (b) where the stress fields at these positions show an elongated and close to round shape, respectively. It is worth noting that both tensile (low wavenumbers – darker areas) and compressive (higher wavenumbers – brighter areas) stresses are present close to subgrain boundaries (marked with a closed black line) with respect to a position which is assumed to be not affected by the stress field of the subgrain boundaries (marked with a star). These inhomogeneous stress states correlate to the distribution of dislocations forming subgrain boundaries. This can be clearly seen in the SEM picture taken on the same area displayed in Figure 4 (a).

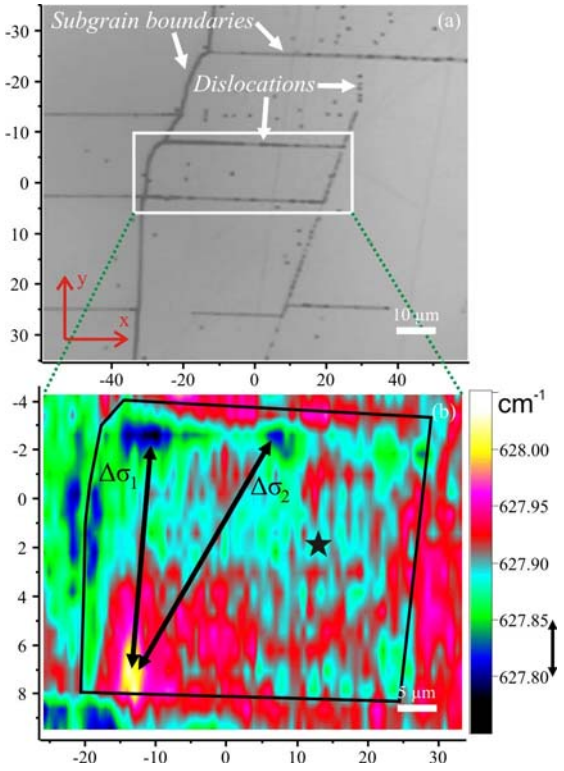

Figure 1: (a) Optical micrograph of the surface of a block-cast mc silicon wafer after mechanical polishing of the SiN antireflective layer and defect etching. Isolated dislocations within subgrains and dislocations forming subgrain boundaries are visible in form of etch pits. (b) One of the three mappings of the relative Raman silicon frequency shifts (cm^{-1}) measured with polarization settings for incident and scattered light showing localized stress fields close to subgrain boundaries. The black arrow on the scale bar corresponds to the peak shift resolution of $\pm$ 0.05 cm^{-1} = $\pm$ 12 MPa.

One of the most critical regions in terms of mechanical stability is the triple point junction where extended defects such as grain boundaries intersect. Here very local stress concentrations may develop during heating and cooling processes most likely due to very local temperature gradients combined with particular grain boundary configurations. An example of stress distribution in a grain boundary triple point region is shown in Figure 2 (b). The following stress-tensor gradient was determined in the right-hand side grain:

$$\Delta\sigma_1 = \begin{pmatrix} -23\pm10 & 5\pm1 & 0 \\ 5\pm1 & -22\pm10 & 0 \\ 0 & 0 & -25\pm10 \end{pmatrix} \text{MPa.}$$

The three grains can be well distinguished in the Raman intensity map displayed in the inset of Figure 2 (a) due to their different Raman scattering efficiency caused by their different crystallographic orientations with respect to the polarization of the incident light [9]. Thus, by correlating the Raman intensity pattern to the optical microscope image one can assign the measured local stresses to the sample's microstructure.

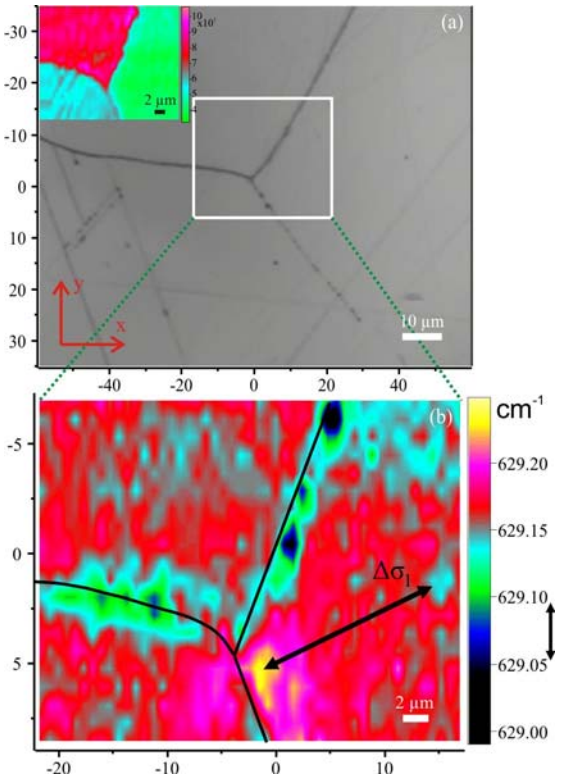

Figure 2: (a) Optical micrograph of the surface of a block-cast mc silicon wafer after mechanical polishing of the SiN antireflective layer and defect etching showing a grain boundary triple point. (inset) The three grains can be distinguished in the Raman intensity map due to their different Raman scattering efficiency. (b) The corresponding mapping of the relative Raman silicon frequency shifts (cm^{-1}) without polarization settings for incident and scattered light. The stress-tensor gradient in the right-hand side grain was determined using polarized µ-Raman spectroscopy.

Figure 3 (b) shows the stress distribution in an area with high concentration of defects containing subgrain boundaries and dislocations within the same grain as confirmed by the Raman intensity mapping (not shown). The subgrain boundaries in this area seem to be formed by merging of individual dislocations [see Figure 4 (b)]. In this case the nucleation of dislocations is considered to take place during the solidification process to relieve totally or partly the stresses produced by the inhomogeneous temperature gradients within the block and/or around inclusions with different thermal expansion coefficient than that of the surrounding silicon [3,8]. These inclusions are not always visible and it is supposed that they are located underneath the surface in the middle of the dislocation area [8]. Thus, the remaining stress fields that could not be reduced by dislocation formation are measured by µ-Raman spectroscopy. It can be seen in Figure 3 (b) that a higher density of defects results in more compressive stress (red – bottom half) relative to a less defective area (green – upper half).

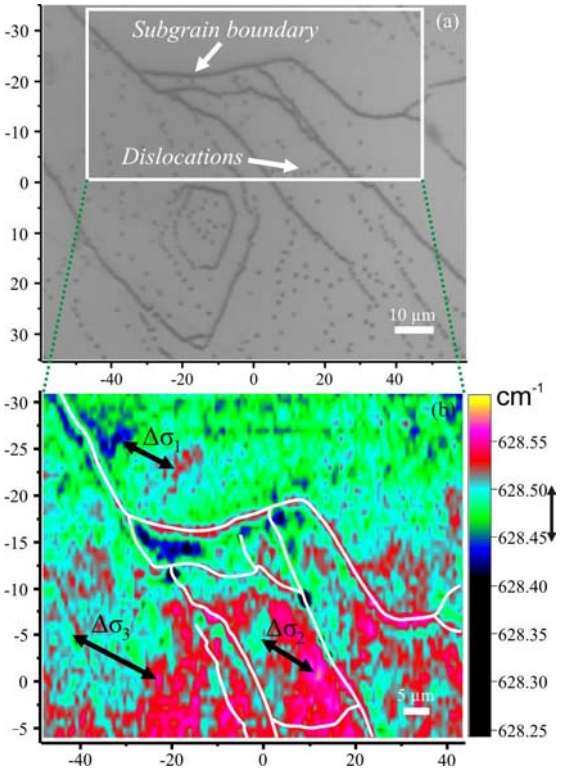

Figure 3: (a) Optical micrograph of the surface of a block-cast mc silicon wafer after mechanical polishing of the SiN antireflective layer and defect etching showing a high defective area. (b) Mapping of the relative Raman silicon frequency shifts (cm^{-1}) without polarization settings. Three average lateral stress gradients $\Delta\sigma_1$=33 $\pm$ 12 MPa, $\Delta\sigma_2$=25 $\pm$ 12 MPa and $\Delta\sigma_3$=20 $\pm$ 12 MPa are obtained applying equation 1. The subgrain microstructure shown in white is inferred from the Raman intensity map.

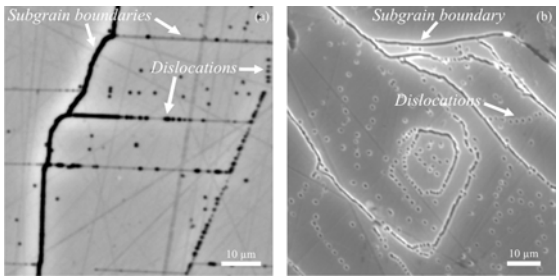

Figure 4: (a, b) SEM images of the same areas shown in Figure 1 (a) and Figure 3 (a), respectively. The different aspect of subgrain boundaries and dislocations results from using different detectors BSE and SE, respectively.

3.2 EFG mc silicon wafers

Figure 5 (a) shows a grain boundary which separates a grain from a region with twin lamellas along with the corresponding mapping of the relative Raman silicon frequency shifts (b) in the area enclosed by the white rectangle. The inhomogeneous stress distribution close to the grain boundary is indicated by two stress gradients $\Delta\sigma_1$ and $\Delta\sigma_2$ corresponding to tensile and compressive stress, respectively, with respect to a position (marked with a star) which is assumed to be not influenced by the stress field close to the grain boundary. Stress gradients can also be present within grains as exemplified by $\Delta\sigma_3$.

The inhomogeneous temperature gradients within the ribbon during the solidification process in connection with grain boundary configurations are considered to be the main source of the measured stress states. To relate stress states at grain boundaries to the orientation of the adjacent grains and thus to the grain boundary type, a combination of µ-Raman and electron backscatter diffraction (EBSD) investigations at identical positions is currently employed.

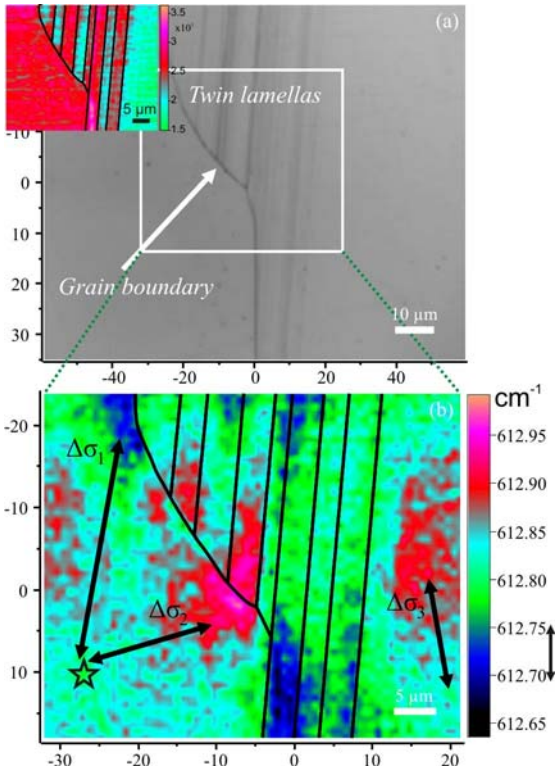

Figure 5: (a) Optical micrograph of the surface of an EFG mc silicon wafer after mechanical polishing and defect etching. (b) Mapping of the relative Raman silicon frequency shifts (cm^{-1}) showing an inhomogeneous stress distribution close to the grain boundary ($\Delta\sigma_1$, $\Delta\sigma_2$) and within one grain ($\Delta\sigma_3$). The grain boundary pattern is inferred from the dependence of the Raman intensity shown in the inset of (a) on the crystallographic grain orientation. Three average lateral stress gradients $\Delta\sigma_1$=28 $\pm$ 12 MPa, $\Delta\sigma_2$=28 $\pm$ 12 MPa and $\Delta\sigma_3$=35 $\pm$ 12 MPa obtained using equation 1 are indicated.

In Figure 6 the stress state of a dislocation-free grain boundary (a, c) is contrasted with the stress state of the same grain boundary accompanied by dislocations located mainly on its right-hand side (b, d). While no stress is measured around the defect-free grain boundary, the presence of dislocations change significantly the stress state on both sides of the grain boundary resulting in tensile (blue) and compressive (red) stresses. It can be considered that in this case as compared to Figure 2 and 5 the thermal stress reached the critical value for dislocation formation, thus relieving partly the stress.

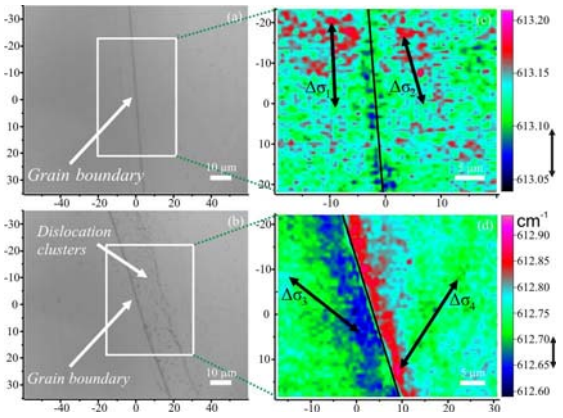

Figure 6: Optical micrograph of the surface of an EFG mc silicon wafer after mechanical polishing and defect etching showing the same grain boundary in a region without (a) and with (b) dislocations. The corresponding mappings (c, d) of the relative Raman silicon frequency shifts (cm^{-1}) reveal that the stress fields close to the grain boundary correlate to the presence of dislocations. Four lateral average stress gradients $\Delta\sigma_1$=$\Delta\sigma_2$=20 $\pm$ 12 MPa, $\Delta\sigma_3$=48 $\pm$ 12 MPa and $\Delta\sigma_4$=53 $\pm$ 12 MPa obtained using equation 1 are indicated.

3.3 LLC mc silicon thin films on glass

The layered laser crystallization (LLC) process used to prepare the mc silicon thin film solar cells on glass is described in [2]. Briefly, in the case of the sample investigated in this paper, a 200 nm thick amorphous hydrogenated silicon (a-Si:H) film deposited by plasma enhanced chemical vapor deposition (PECVD) is crystallized by a single scan of a line focus cw diode laser at a sample holder temperature of 690 ^{o}C to form a seed layer. This layer is epitaxially thickened up to 2.5 µm by a combination of electron beam evaporation of a-Si and repeated crystallization by excimer laser pulses after each ~ 20 nm of newly deposited a-Si. During the epitaxial growth the sample holder temperature was 600 ^{o}C.

Two representative examples of stress distribution in LLC mc silicon thin films on borosilicate glass are shown in Figure 7. Both the seed and the epitaxial thickened layers are probed. The mechanisms of stress formation and relaxation during the laser melting and re-crystallization of the a-Si:H seed layer on glass are not yet fully understood. The exact temperature of the borosilicate glass substrate during crystallization is not known, the lower limit being the sample holder temperature of 690 ^{o}C. Above this temperature the borosilicate glass is soft enough (strain point 518 ^{o}C, softening point 820 ^{o}C) to partially or totally incorporate the stress present in the seed layer [6,10,11]. During the cooling process the seed layer is largely preventing from contracting by the substrate due to a higher thermal expansion coefficient of the crystalline silicon than that of the borosilicate glass substrate down to ~ 135 ^{o}C [12].

This results in tensile (thermal) stress in the seed layer originating from the glass-silicon interface at room temperature [6,11]. A part of this stress is transferred to the substrate when the sample holder is heated up to 600 ^{o}C for the epitaxial thickening step.

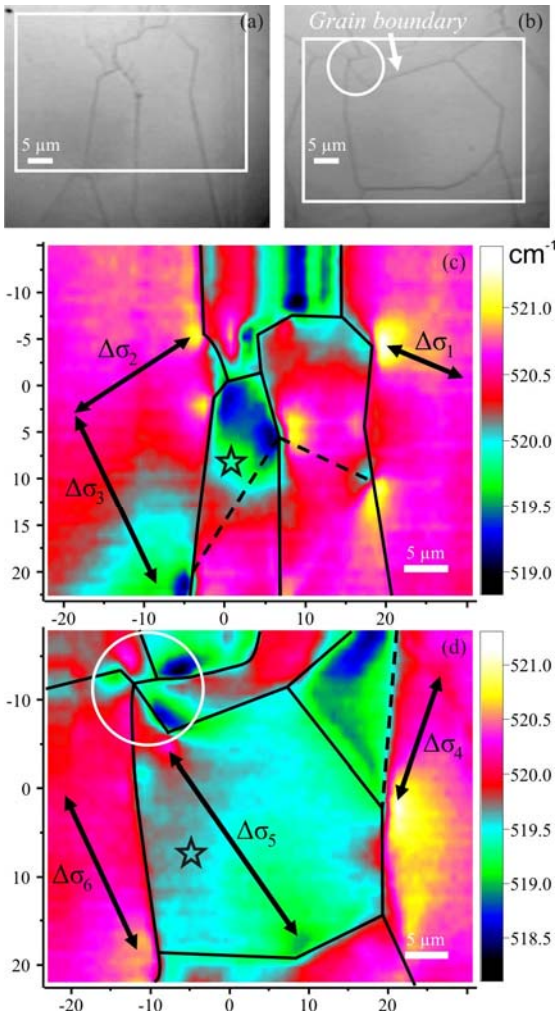

Figure 7: (a, b) Optical images of the surface of an LLC mc silicon thin film solar cell on glass after mechanical polishing and defect etching. Since the defect etching time was only 5s not all grain boundaries and dislocation may become visible in form of pits in the optical images. The white circle marks a multiple grain boundary junction area, while the rectangles mark the µ-Raman investigated areas. (c, d) Mappings of the absolute Raman silicon frequency shifts (cm^{-1}) showing an overall tensile stress except close to convex and concav grain boundary tips and multiple grain boundary junctions where localized and extended stress distributions including both compressive and tensile contributions are present. The stars mark two grains whose stress states are influenced by the shape of their boundaries. The dashed lines in the grain boundary pattern are not visible in the optical images being inferred from the dependence of the Raman intensity on the crystallographic grain orientation. Six average lateral stress gradients ($\pm$ 12 MPa) obtained using equation 1 are indicated $\Delta\sigma_1$=157, $\Delta\sigma_2$=52, $\Delta\sigma_3$=$\Delta\sigma_4$=227, $\Delta\sigma_5$=300 and $\Delta\sigma_6$=129 MPa.

Following the same reasoning as for the seed layer it is reasonable to assume that tensile stress is produced in the epi-layer during the cooling process due to the temperature gradient resulting in different thermal expansion coefficients between the newly and previously crystallized silicon layers. The presence of an overall tensile stress except close to certain grain boundary configurations is confirmed by the shift of the absolute Raman silicon peak to lower wavenumbers with respect to that of a single crystalline silicon wafer at ~ 520.9 cm^{-1} which is often used as a stree-free reference (see Figure 7). Microstructure induced compressive and tensile stresses were found close to convex and concav grain boundary tips and multiple grain boundary junctions. The stress fields can be either localized ($\Delta\sigma_1$, $\Delta\sigma_2$) or extended ($\Delta\sigma_3$) as seen in Figure 7 (c). A critical area with respect to mechanical stability is the multiple grain boundary junction area marked with a circle in Figure 7 (b, d). It can be considered that the presence of both tensile and compressive stresses around this area ensures its mechanical stability. The stress distribution within smaller grains such as those marked with a star in Figure 7 (c, d) was found to be influenced by the shape of their boundaries.

4 CONCLUSIONS

The residual local stresses present at critical positions in multicrytalline silicon solar cells based on block-cast and edge-defined film-fed growth wafers and layered laser crystallized thin films on glass have been investigated by micro-Raman spectroscopy. These stresses are considered to be produced during heating and cooling processes due to inhomogeneous temperature gradients combined with particular grain boundary configurations. In the case of block-cast and EFG wafers, inhomogeneous stress distributions including both compressive and tensile stresses were found at (1) subgrain boundaries depending on the distribution of dislocations forming them, (2) a grain boundary triple point, (3) a highly defective area within a grain, (4) a grain boundary separating a grain from a region with twin lamellas and (5) a grain boundary accompanied by dislocations. The LLC thin films on glass are stressed in tension with respect to a stress-free single crystalline silicon wafer except close to convex and concav grain boundary tips and multiple point junctions where inhomogeneous stress distributions were measured. The stress distribution within smaller grains was found to be influenced by the shape of their boundaries. Polarized µ-Raman spectroscopy can be used to obtain 3D stress distributions with a lateral and in-depth resolution depending on the objective and the excitation wavelength used.

5 ACKNOWLEDGMENTS

This work was financially supported by the German Federal Ministry for the Environment, Nature Conservation and Nuclear Safety and all the industry partners within the research cluster SolarFocus (0327650D) and by the European Commission within the FP7-Energy project “High-EF”. The authors would like

to thank F. Falk for fruitful discussions and A. Gawlik of IPHT for carrying out the LLC processing.

6 REFERENCES

[1] P. J. Withers, Rep. Prog. Phys. 70 (2007) 2211.
[2] G. Andrä, J. Bergmann, A. Bochmann, F. Falk, S. Dauwe, T. Kieliba, 20th European Photovoltaic Solar Energy Conference, Barcelona, (2005) 1171.
[3] M. Becker, H. Scheel, S. Christiansen, and H. P. Strunk, J. Appl. Phys. 101 (2007) 063531.
[4] F. Secco D' Aragona, J. Electrochem. Soc. 119 (1972) 948.
[5] I. De Wolf, Semicond. Sci. Technol. 11 (1996)139.
[6] G. Sarau, M. Becker, A. Berger, J. Schneider, and S. Christiansen, Mater. Res. Soc. Symp. Proc. 1024E (2007) 1024-A07-04.
[7] H. Nordmark, M. Di Sabatino, E. J. Øvrelid, J. C. Walmsley and R. Holmestad, Proceedings 22nd European Photovoltaic Solar Energy Conference, Milan, (2007) 1710.
[8] B. Ryningen, K. S. Sultana, E. Stubhaug, O. Lohne, P. C. Hjemås, Proceedings 22nd European Photovoltaic Solar Energy Conference, Milan, (2007) 1086.
[9] S. Kouteva-Arguirova, W. Seifert, M. Kittler, J. Reif, Mater. Sci. Eng. B 102 (2003) 37.
[10] J. Schneider, S. Christiansen, Ch. Genzel, Proceedings 22nd European Photovoltaic Solar Energy Conference, Milan, (2007) 2001.
[11] P. Lengsfeld, N. H. Nickel, Ch. Genzel, and W. Fuhs, J. Appl. Phys. 91 (2002) 9128.
[12] M. Okaji, Int. J. Thermophys. 9 (1988) 1101.